A Parameter Estimation Framework for Patient-Specific Assessment of Aortic Coarctation

4

Lucian Itu, Puneet Sharma, Tiziano Passerini, Ali Kamen, and Constantin Suciu

Abstract

In this chapter we introduce a method based on computational fluid dynamics for non-invasively assessing patients with aortic coarctation. While in practice the pressure gradient across the coarctation is typically measured invasively with a catheter, the proposed method determines the pressure gradient using a computational modeling approach, which relies on medical imaging data, routine non-invasive clinical measurements and physiological principles. The main components of the method are a reduced-order model coupled with a comprehensive pressure-drop formulation, and a parameter estimation method for personalizing the boundary conditions and the vessel wall parameters. The parameter estimation method is fully automated, and is based on an iterative tuning procedure to obtain a close match between the computed and the non-invasively determined quantities. A key feature is a warm-start to the optimization procedure, with better initial solution for the nonlinear system of equations, to reduce the number of iterations needed for the calibration of the geometrical multiscale models. To achieve these goals, the initial solution, computed with a lumped

Large parts of Sects. 4.2, 4.3 and 4.4 have been published before in the paper 'A Parameter Estimation Framework for Patient-specific Hemodynamic Computations', Journal of Computational Physics, Volume 281, 15 January 2015, Pages 316–333.

L. Itu (✉) • C. Suciu
Corporate Technology, Siemens SRL, B-dul Eroilor nr. 3A, Brasov 500007, Romania

Automation and Information Technology, Transilvania University of Brasov, Mihai Viteazu nr. 5, Brasov 5000174, Romania
e-mail: lucian.itu@siemens.com

P. Sharma • T. Passerini • A. Kamen
Medical Imaging Technologies, Siemens Healthcare, 755 College Road, Princeton, NJ 08540, USA

L.M. Itu et al. (eds.), *Patient-specific Hemodynamic Computations: Application to Personalized Diagnosis of Cardiovascular Pathologies*,
DOI 10.1007/978-3-319-56853-9_4

parameter model, is adapted before solving the parameter estimation problem for the geometrical multiscale circulation model: the resistance and the compliance of the circulation model are estimated and compensated. This feature is based on research, and is not commercially available. Due to regulatory reasons its future availability cannot be guaranteed.

4.1 Introduction

Aortic coarctation (CoA) represents a congenital cardiac pathology which is encountered in 5–8% of the patients with congenital heart pathologies (Ringel and Jenkins 2007). Its luminal appearance is similar to that of an atherosclerotic stenosis: a local narrowing of the aortic wall. Different methods are used for assessing the CoA severity: the anatomy is typically assessed using Magnetic Resonance Imaging (MRI) or Computed Tomography (CT). The functional assessment of aortic coarctations is based on the pressure drop along the CoA. The gold standard for determining the pressure drop is invasive catheterization. Due to the costs and the risks associated with this invasive procedure, other less accurate methods have also been proposed. The velocities measured using Doppler echocardiography are used in the simplified or modified Bernoulli equations to determine the pressure drop, but, on one hand, these velocities are sometimes difficult to measure due to the placement of the descending aorta, and, on the other hand, the computed values often overestimate the actual gradient (Seifert et al. 1999). The difference between cuff-based blood pressure measurements performed at the arms and legs represents another simple, non-invasive and cost-effective method, but is also unreliable (Hom et al. 2008).

To address this issue, Computational Fluid Dynamics (CFD) based blood-flow models have been proposed for analyzing the hemodynamics in idealized and/or patient-specific healthy and diseased aortic geometries. These models provide important insights into the structure and function of the cardiovascular system, and have been proposed in recent years, for diagnosis, risk stratification, and surgical planning (Cebral et al. 2011; Haggerty et al. 2013; Quarteroni et al. 2000; Taylor and Steinman 2010).

Different approaches have been proposed for specifying the outlet boundary conditions, ranging from pressure or flow rate profiles to lumped parameter models (0D models). For an accurate patient-specific computation, the role of physiologically sound boundary conditions is well appreciated in the literature. The effect of distal vasculature is modeled by outlet boundary conditions coupled with the computational domain (region of interest), resulting in a geometrical multiscale model. The boundary conditions are represented by lumped parameter models, which are designed to capture one (or more) of the (1) total resistance, (2) total compliance, and (3) the wave propagation and reflection effects in the distal vasculature. The most widely used lumped parameter model is the three-element windkessel model (Westerhof et al. 2009), which is characterized by its simplicity (only three parameters), and ability to capture two important characteristics of the distal circulation (compliance and resistance).

In a clinical scenario, the values of the windkessel model parameters are not available on a per-patient basis. Instead, multiple pressure or flow measurements are

usually available for each patient. A clinically feasible and accurate flow computation should not only be in agreement with these measurements, but should also have means to model other hemodynamic states for the same patient. To achieve this, one has to estimate a set of personalized windkessel model parameters, while ensuring that the computations match the measured data.

Different calibration procedures for the outlet boundary conditions have been proposed. Olufsen et al. proposed a calibration method for determining the dynamic cerebral blood flow response to sudden hypotension during posture change (Olufsen et al. 2002). Their experimental calibration procedure depends strongly on the patient-specific state, i.e. on the position of the patient.

A fully automatic optimization-based calibration method for the windkessel models was suggested (Spilker and Taylor 2010), where the input was specified by non-invasively acquired systolic/diastolic pressures and, in some cases, additional flow data. The windkessel parameters were obtained by solving a system of nonlinear equations, formulated based on a set of objectives for the pressure and flow rate waveforms at various locations. A Broyden method was employed for solving the nonlinear system of equations. The initial parameter values were determined by a reduced-order model, composed of only the windkessel models of the geometrical multiscale model.

An adjoint based method for calibrating the windkessel parameters was proposed (Ismail et al. 2013a, b), where the Jacobian was computed without the use of finite-differences, and eliminated the risk of that the Broyden's method would not converge for initial guesses far away from the solution. Furthermore, a reduced-order model with resistance outlet boundary conditions was introduced (Blanco et al. 2012), under which the terminal resistance values of the arterial model of the arm were adapted to obtain desired flow rate distribution between vascular territories.

A competitive alternative to the above mentioned optimization based methods is represented by filtering based methods. These methods were successfully used to estimate different aspects of fluid-structure interaction applications, like arterial wall stiffness (Pant et al. 2014), the surrounding tissue support (Moireau et al. 2013), or windkessel parameters (Bertoglio et al. 2012).

Herein we propose a parameter estimation method for personalizing hemodynamic computations (Itu et al. 2015). The proposed method is inspired by the approach introduced previously (Spilker and Taylor 2010), and has been developed based on the following strategies: a warm-start of the optimization procedure with better initial solution, and a reduction in the number of iterations performed for the calibration of the geometrical multiscale models (for simplifying phrasing, we will refer to geometrical multiscale models simply as multiscale models). The first strategy aims at reducing the risk of a possible failure of the optimization approach due to a bad initial guess (Ismail et al. 2013a, b)—a fairly common occurrence for pathologic cases. Moreover, we can achieve a faster computation time for the overall estimation method by reducing the number of repetitive iterations on the same geometry.

The parameter estimation method automatically determines the windkessel parameters in the multiscale circulation model, by solving a system of nonlinear equations. To obtain an initial guess, the equations are first solved for a lumped parameter model. The main characteristic of the proposed method is that, when

switching from the lumped model to the multiscale model, the windkessel parameters are appropriately adapted to take into account the hemodynamic properties (resistance and compliance) of the multiscale model.

The concepts and information presented in this chapter are based on research and are not commercially available. Due to regulatory reasons its future availability cannot be guaranteed.

4.2 Methods

In this section, we describe an efficient optimization-based algorithm, which ensures that the personalized flow computations are in close agreement with the physiological measurements. In the present study, we use a 1D–0D reduced-order geometrical multiscale model as proof of concept. One-dimensional models have been shown to accurately predict time-varying flow rate and pressure wave forms (Reymond et al. 2011). Most of the one-dimensional models introduced in literature use elastic wall laws (Stergiopulos et al. 1992; Olufsen et al. 2000; Formaggia et al. 2003; Mynard and Nithiarasu 2008), but viscoelastic arterial wall models have also been applied (Alastruey et al. 2011; Malossi et al. 2012). Further, recent research activities have shown the growing interest in the one-dimensional blood flow model not only for the computation of a full body arterial model, but also for specific parts of the circulation in pathologic situations: the coronary circulation (Itu et al. 2012), the abdominal aorta (Raghu et al. 2011; Low et al. 2012), proximal part of the aorta (Itu et al. 2013), and the aortic valve (Mynard et al. 2012). The 1D model used in this study has been previously introduced in (Itu et al. 2012, 2013). Time-varying flow rate profiles are used as inlet boundary condition, while three-element windkessel models were coupled at the outlets of the highest order model. The 3-element windkessel model is represented by the following relationship between instantaneous flow and pressure:

$$\frac{dp}{dt} = R_p \frac{dq}{dt} - \frac{p}{R_d \cdot C} + \frac{q\left(R_p + R_d\right)}{R_d \cdot C}, \tag{4.1}$$

where p is the instantaneous pressure at the inlet of the windkessel model, q is the instantaneous flow rate, R_p and R_d are the proximal and distal resistance respectively, and C is the compliance.

Next, we briefly review the calibration method proposed previously and introduce the proposed parameter estimation method.

4.2.1 Calibration Method for Windkessel Parameters

The calibration method automatically estimates the free parameters (windkessel parameters) to ensure that the computed pressure and flow-rate values minimize the objective function (Spilker and Taylor 2010). More specifically, the algorithm iteratively

estimates the total resistance of the windkessel model, R_t, the proximal resistance ratio, ρ, and the time constant of the exponential pressure decay in the windkessel model at zero flow, τ:

$$R_t = R_p + R_d, \tag{4.2}$$

$$\rho = R_p / R_t, \tag{4.3}$$

$$\tau = R_d \cdot C. \tag{4.4}$$

Measured pressure and/or flow rate values are used as objectives of the calibration method. The parameter estimation problem is formulated as a solution to a system of nonlinear equations, with each equation representing the residual error between the computed and measured quantity of interest. To determine the values of all the residuals ($\boldsymbol{f}(\boldsymbol{x}_i)$), a computation with the parameter values $\boldsymbol{x}_i$ is required. Since the absolute values of the adapted parameters and of the residuals generally differ by orders of magnitude, for the calibration method both the parameter and the objective residuals have been scaled using typical values, as is described below.

The nonlinear system of equations is first solved for a 0D model, composed of the windkessel models used in the multiscale model. To find an initial solution for the 0D model, a grid of physiological parameter value sets is considered. The parameter value set leading to the smallest L_2 norm for the objective residual, is used as initial solution for a dogleg trust region method, which determines the solution $\boldsymbol{x}_0$ used during the subsequent steps.

Next, a fixed-point approach is used to compute a finite-difference Jacobian which is determined using the typical step sizes, and is consistent with the chosen typical values of the objective residuals. The components of the Jacobian approximations are computed as follows:

$$J_{ij} = \frac{1}{s_j^{typ}}\left[\mathbf{f}\left(\mathbf{x}_0 + \frac{1}{2}s_j^{typ}\mathbf{e}_j\right) - \mathbf{f}\left(\mathbf{x}_0 - \frac{1}{2}s_j^{typ}\mathbf{e}_j\right)\right]\cdot\mathbf{e}_i, \tag{4.5}$$

where $\boldsymbol{e}_i$ and $\boldsymbol{e}_j$ represent the unit vectors in the ith and jth direction respectively, and s_j^{typ} is the typical step size for parameter j, given by:

$$s_j^{typ} = 1\Big/\sqrt{\sum_{i=1}^{n_{eq}}\left(J_{ij} / f_i^{typ}\right)}, \tag{4.6}$$

where f_i^{typ} is the typical value of the objective residual f_i.

The process composed of Eqs. (4.5) and (4.6) is an iterative procedure which is terminated once the Euclidian norm of the difference of two consecutive Jacobians, normalized by the corresponding f_i^{typ} and s_j^{typ} values, is less than 10^{-6}.

Next, the multiscale model is set up and run, and the objective residuals are evaluated. For the first run with the multiscale model, the solution variables are initialized based on the results obtained with the 0D model. Each computation, with a given set

of parameter values, is run until the L_2 norms of the normalized differences between the pressure and flow rate profiles at the current and the previous cardiac cycle are smaller than 10^{-5}.

If all objective residuals are smaller than the tolerance limit (taken here equal to $f_i^{typ}/10$), the calibration method is terminated. Otherwise, a quasi-Newton method is employed to update the parameter values. First the Jacobian matrix is updated: since the computation of a finite-difference Jacobian matrix with the multiscale model is expensive, the Jacobian determined with the fixed-point approach is updated at each iteration, using:

$$\mathbf{J}_{i+1} = \mathbf{J}_i + \frac{\left[\mathbf{f}\left(\mathbf{x}_{i+1}\right) - \mathbf{f}\left(\mathbf{x}_i\right) - \mathbf{J}_i\mathbf{s}_i\right]\left(\mathbf{D}_s^2\mathbf{s}_i\right)^T}{\mathbf{s}_i^T\mathbf{D}_s^2\mathbf{s}_i}, \tag{4.7}$$

where $\mathbf{s}_i = \mathbf{x}_{i+1} - \mathbf{x}_i$ is the current step and $\boldsymbol{D}_s$ is a diagonal scaling matrix:

$$\left(D_s\right)_{ij} = \begin{cases} 1/s_j^{typ}, & i = j \\ 0, & i \neq j \end{cases} \tag{4.8}$$

Finally, the new parameter values are estimated:

$$\mathbf{x}_{i+1} = \mathbf{x}_i - \mathbf{J}_i^{-1}\mathbf{f}\left(\mathbf{x}_i\right). \tag{4.9}$$

The main drawback of the above described calibration method is that the hemodynamic properties of the highest order model of the multiscale model are not taken into account when switching from the 0D model to the multiscale model. This aspect has several consequences. First of all, the solution obtained for the 0D model, which is used as initial solution for the nonlinear system of equations solved for the multiscale model, is considerably different from the final solution of the parameter values. This can lead to a failure of the minimization approach employed for the nonlinear system. Furthermore, this risk is enhanced when the hemodynamic computation is performed for pathologic cases, i.e. when the hemodynamic properties of the highest order model become more important compared to the properties of the 0D model. Secondly, the number of calibration iterations required to obtain the final solution for the parameter values increases. These repetitive computations increase the total execution time, an aspect which is a significant disadvantage when the calibration method is applied for patient specific computations in a clinical setting.

4.2.2 Proposed Parameter Estimation Framework

We introduce a parameter estimation method which eliminates the drawbacks of the calibration method described in the previous section. An outline of the algorithm is illustrated in Fig. 4.1, which is composed of the steps described previously and two critical steps (displayed in bold: steps 6 and 7). One of the main advantages of the proposed algorithm is that it can be efficiently applied not only for healthy cases, but also for pathologic cases. The main idea is to efficiently account for the hemodynamic

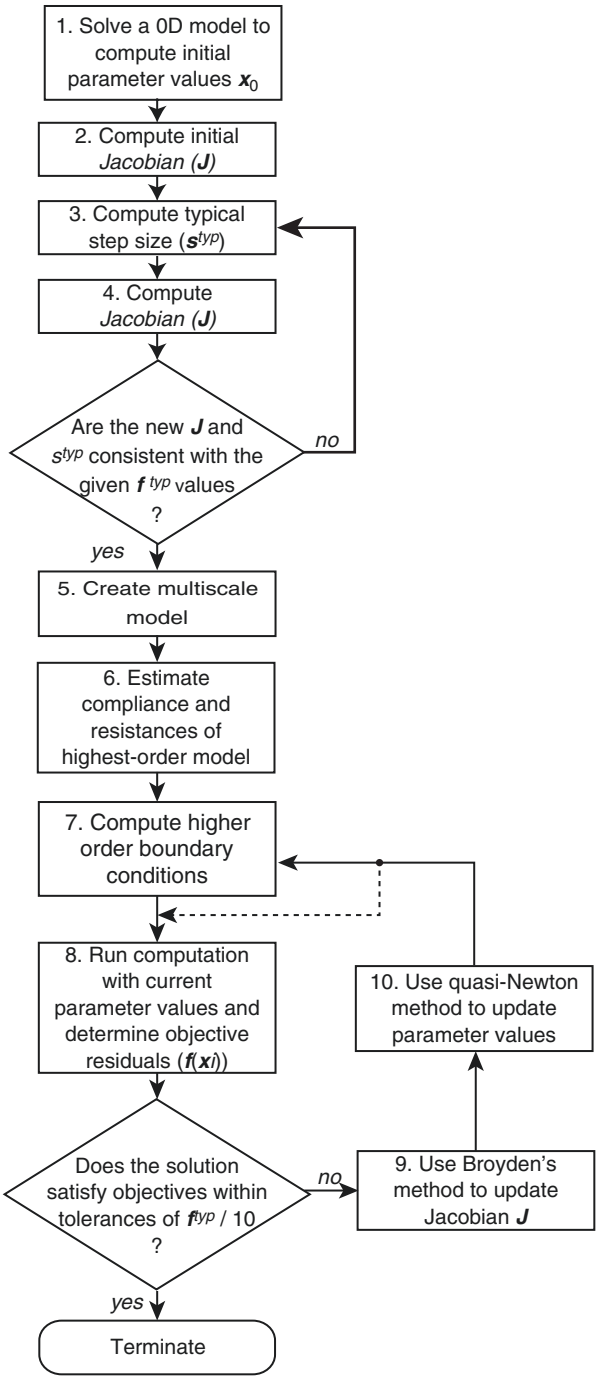

Fig. 4.1 The proposed parameter estimation method (Itu et al. 2015)

properties of the highest order model inside the multiscale model, when switching from the 0D model to the multiscale model. Particularly, we focus on two properties of the multiscale model: the compliance and the resistance.

At step 6, the compliance and resistances of the highest order model are estimated. These two quantities have not been taken into account when solving the nonlinear system of equations with the 0D model. Next, at step 7, the parameter values of the windkessel models are recomputed to account for the hemodynamic properties of the highest order model. Note that the values of the parameters of the nonlinear system are not modified at this stage and only the windkessel parameters are changed. The algorithms used for the estimation and compensation of the resistances and compliances are described in the next two subsections.

As a result of the two additional steps, the parameter estimation method adapts the overall properties of the multiscale models. For the multiscale computation, the windkessel parameters are the only quantities updated from one iteration to the next.

The parameter estimation methods do not always use the total resistances or the compliances as calibrated parameters. Nevertheless, regardless of the choice of parameters, the resistances and the compliances of the terminal windkessel models are always adapted when switching from the 0D model to the multiscale model. Additionally, if the resistances or the compliance of the multiscale model are adapted directly or indirectly, the parameters of the windkessel models are recomputed at the end of each iteration, based on the new parameter values determined through Eq. (4.9) and the estimated quantities of the highest order model. If the quantities are not adapted at all, then step 7 is applied only once (an aspect indicated by the dashed line in Fig. 4.1). The target objectives are: maximum pressure, P_{max}, minimum pressure, P_{min}, and flow rate split between outlets of the highest order model, Φ. The typical value of the residuals for pressure and flow-rate split objectives was set to 1 mmHg and 0.005 respectively.

4.2.3 Resistance Estimation and Compensation

To estimate the resistance of a healthy vascular segment for the highest order model, $(R_{HO})_i$, we assume a velocity profile:

$$\left(R_{HO}\right)_i = \frac{2\left(\gamma+2\right)\mu}{\pi}\int_0^{L_i}\frac{1}{r_i^4\left(l\right)}dl \tag{4.10}$$

where γ is the power coefficient in the velocity profile $u = \bar{U}\frac{\gamma+2}{\gamma}\left[1-\left(\frac{r}{R}\right)^{\gamma}\right]$, μ is the viscosity and r_i is the radius. For this work, we have chosen a parabolic profile ($\gamma = 2$) without any loss of generality. Alternatively a power law profile ($\gamma = 9$) or a Womersley profile can be considered (Womersley 1955).

For a pathologic vascular segment (e.g. coarctation, stenosis) we use a comprehensive pressure-drop model to estimate the resistance of the pathological segment.

This approach was validated against catheter-based ground-truth measurements in our previous work (Itu et al. 2013). Since the time-varying flow rate through the descending aorta is not known apriori, the resistance of the CoA segment is computed from the average flow rate (which represents an objective of the parameter estimation method, i.e. it is known apriori):

$$\left(R_{HO}\right)_i = R_{CoA}\left(Q\right) = \Delta P\left(\bar{Q}_{DAo}\right) / \bar{Q}_{DAo}, \tag{4.11}$$

where $\Delta P(\bullet)$ refers to the pressure drop model (Itu et al. 2013), and $\bar{Q}_{DAo}$ is the average flow rate through the descending aorta.

A similar approach can also be used if the multiscale model contains stenosed arteries. Depending on the region of interest, different pressure drop models have been proposed in the literature, e.g. coronary artery stenosis (Huo et al. 2012), femoral artery stenosis (Young et al. 1975), renal artery stenosis (Steele 2007). For aneurysms, a different pressure drop model (Bessems 2007) can be applied to estimate the resistance.

Equations (4.10)/(4.11) are used at step 6 in Fig. 4.1 to determine the resistance of each branch of the multiscale model. Next, we introduce a recursive algorithm, employed at step 7, for adapting the total terminal resistances of the windkessel models, which is used during the switch from the 0D model to the multiscale model. Let n be the number of outlets in the geometric model, $(R_{t-0D})_j$ represents the total (sum of proximal and distal) resistance of the windkessel model used at each outlet ($j = 1 \ldots n$). The objective is to estimate the total resistances at each outlet of the geometric multiscale model $(R_{t-MS})_j$. Algorithm 1 illustrates the recursive function used for the resistance adaptation.

Algorithm 1: *adaptResistance* (totalRes, vesselNr)

$R_t \leftarrow$ totalRes
$i \leftarrow$ vesselNr
$(R_{t-MS})_i \leftarrow R_t - (R_{HO})_i$
if vessel i is a terminal vessel
return
else

$$\left(R_{t-0D}\right)_i \leftarrow 1 \Big/ \sum_k \frac{1}{\left(R_{t-0D}\right)_k}, \quad k \rightarrow \text{terminal vessels downstream from vessel } i$$

for each daughter vessel j of vessel i
$\Phi_j \leftarrow (R_{t-0D})_i / (R_{t-0D})_j$
$(R_{t-MS})_j \leftarrow (R_{t-MS})_i / \Phi_j$
adaptResistance $((R_{t-MS})_j, j)$
end (for)
end (if)
return

The function *adaptResistance* is called exactly once for the root segment of the arterial tree, which recursively computes all terminal resistances of the

multiscale model. If the current segment is a terminal segment, the total terminal resistance is determined by subtracting the multiscale resistance of the current segment from the total resistance at the root of the vessel. If the current segment has daughter vessels, the goal is to distribute the new total resistance, $(R_{t-MS})_i$, to the outlets of segment i, in a manner that maintains the flow rate ratio in each daughter vessel. In the first step, the total resistance of the daughter vessels inside the 0D model is determined. Next, for each daughter vessel, using the ratio of total resistance of current vessel to terminal resistance of the current daughter vessel (Φ_j), the new terminal resistance of the current daughter vessel is determined ($(R_{t-MS})_j$). If the daughter vessel j is not a terminal vessel, $(R_{t-0D})_j$ is computed using the resistances of the downstream terminal vessels. Finally, function *adaptResistance* is called to further distribute the resistance of the current daughter vessel.

Equations (4.10)/(4.11) are used to estimate only once the resistance of each vascular segment. If the resistances are adapted directly or indirectly, Algorithm 1 is also applied, in a slightly modified version, at the end of each calibration iteration performed for the multiscale model (after computing the new parameter values through Eq. (4.9)). Hence, the total resistances of the 0D model used in Algorithm 1, $(R_{t-0D})_j$, are substituted by the total equivalent resistances of the multiscale model at each outlet of the highest order model, $(R_t)_j$, which is determined before applying the modified version of Algorithm 1. If the directly or indirectly adapted resistance refers to a single outlet, $(R_t)_j$ is set equal to this parameter value. Otherwise the parameter value is distributed to all outlets covered by the parameter. For the current study, we use a power law:

$$\left(R_t\right)_j = R_t \cdot \sum_k r_k^m \Big/ r_j^m, \tag{4.12}$$

where R_t refers to the adapted parameter, index k is used to iterate over all outlets covered by the adapted parameter and m is a power coefficient, whose physiological range of values is between two for large arteries (Zamir et al. 1992) and three for small arteries (Murray 1926).

4.2.4 Compliance Estimation and Compensation

To estimate the compliance of a vascular segment i of the highest order model in the multiscale model, $(C_{HO})_i$, we use the material properties of the arterial wall:

$$\left(C_{HO}\right)_i = \int_0^{L_i} \frac{3\pi r_i^2(l)}{2} \cdot \frac{r_i(l)}{E_i \cdot h_i} dl, \tag{4.13}$$

where E_i is the Young's modulus and h_i is the wall thickness. Most of the compliance in an arterial/venous tree resides in the large vessels, hence the compliance of the highest order model may become significant compared to the compliance of the windkessel elements, especially when using domains with large arteries. Next, the

total compliance of the highest order model is determined $C_{HO} = \sum_i \left(C_{HO}\right)_i$, which is then distributed to the outlets of the geometric model:

$$\left(C_{MS-a}\right)_j = \left(C_{HO} \cdot r_j^2\right) \Big/ \sum_{j=1}^{n} r_j^2 , \tag{4.14}$$

where $(C_{MS-a})_j$ represents the assumed additional compliance introduced at each outlet of the highest order model inside the multiscale model. The goal is to determine the compliance of the windkessel models, $(C_{MS})_j$, so as to obtain for the multiscale model the same total compliance as the one used for the 0D model, $(C_0D)_j$. Figure 4.2 introduces different representations for the compliance of the multiscale model, alongside the 0D model.

Figure 4.2a displays the classic representation of the multiscale model, composed of the highest order model and the terminal windkessel element. In Fig. 4.2b, the compliance of the highest order model is lumped into a 0D compliance at outlet j, $(C_{MS-a})_j$, placed before the windkessel model. To determine the compliances of the windkessel elements of the multiscale model, $(C_{MS})_j$, $(C_{MS-a})_j$ is ported inside the windkessel model, as displayed in Fig. 4.2c. For the models in Fig. 4.2c, d to be equivalent, the following relationship must hold:

$$\left(C_{MS}\right)_j = \left(C_{0D}\right)_j - \left(C_{MS-a-WK}\right)_j \tag{4.15}$$

Hence, to determine $(C_{MS})_j$, $(C_{MS-a-WK})_j$ must be computed. $(C_{MS-a-WK})_j$ represents the assumed additional compliance introduced by the multiscale model at outlet j and ported inside the three-element windkessel model. Three different approaches were tested for computing $(C_{MS-a-WK})_j$.

Approach 1—Direct compliance compensation. The influence of the proximal resistance of the windkessel model is neglected:

$$\left(C_{MS-a-WK}\right)_j = \left(C_{MS-a}\right)_j \tag{4.16}$$

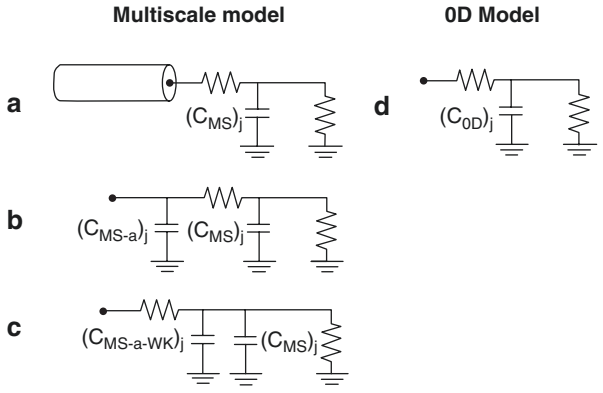

Fig. 4.2 (**a**) Classic representation of the multiscale model; (**b**) the compliance of the highest order model is lumped into a 0D compliance at outlet j placed before the windkessel model; (**c**) the compliance of the highest order model is ported inside the windkessel element; (**d**) classic representation of the windkessel model

Approach 2—Analytical compliance compensation. Approach 1 does not take into account the fact that the proximal resistance of the windkessel element diminishes the influence of the compliance. Thus, following a method proposed previously (Grinberg and Karniadakis 2008):

$$\left(C_{MS-a-WK}\right)_j = \left(C_{MS-a}\right)_j \Big/ \left(1-\left(R_{p-MS}\right)_j / \left(R_{t-MS}\right)_j\right), \tag{4.17}$$

where $(R_{p-MS})_j$ is the proximal resistance of the windkessel model at outlet j of the highest order model.

Approach 3—Numerical compliance compensation. Thirdly, we propose a numerical approach based on the pulse pressure method (PPM) (Stergiopulos et al. 1994), which is described in Algorithm 2. PPM has been introduced to estimate the compliance downstream of a location in an arterial tree, at which the time-varying flow rate values and the average and pulse pressure are known. In the following we use a modified PPM, based on a three-element windkessel model (PPM-WK3) which replaces the two-element windkessel model in the original PPM.

Algorithm 2: PPM-Based Compliance Compensation

for each terminal vessel j

Run computation with two element WK model

$((Q_{0D}(t))_j, (R_{t-MS})_j, (C_{MS-a})_j) \rightarrow (PP_{\text{ref}})j$

Initialize PPM-WK3 $\rightarrow (Q_{0D}(t))_j$, $(R_{p-MS})_j$, $(R_{d-MS})_j$, $(C_{MS-a})_j$,$(PP_{\text{ref}})_j$

Run PPM-WK3 $\rightarrow (C_{MS-a-PPM})_j$

$(C_{MS-a-WK})_j \leftarrow (C_{MS-a-PPM})_j$

end (for)

First, a two-element windkessel model is used to determine a reference pulse pressure, $(PP_{\text{ref}})_j$, using the flow rate profile obtained at outlet j of the highest order model during the last computation performed with the 0D model, $(Q_{0D}(t))_j$, the total resistance at outlet j after resistance compensation, $(R_{t-MS})_j$, and the assumed additional compliance introduced at outlet j, $(C_{MS-a})_j$. Next, PPM-WK3 is initialized and run, and as a result the compliance value, to be subtracted in Eq. (4.15) from the compliance used inside the 0D model, is determined.

Approaches 1–3 are used to estimate only once the assumed additional compliance introduced by the multiscale model at each outlet j of the highest order model. If the compliance of the multiscale model is adapted directly or indirectly, the compliance values of the windkessel elements are recomputed at each calibration iteration performed for the multiscale model. In this case, considering C the total compliance of the multiscale model, this value is first distributed to the outlets of the highest order model, using a relationship similar to Eq. (4.14):

$$\left(C_{MS-t}\right)_j = \left(C \cdot r_j^2\right) \Big/ \sum_{j=1}^{n} r_j^2, \tag{4.18}$$

where $(C_{MS-t})_j$ represents the total equivalent compliance of the multiscale model at each outlet of the highest order model.

For the recomputation of the windkessel compliance, a relationship similar to Eq. (4.15) is employed:

$$\left(C_{MS}\right)_j = \left(C_{MS-t}\right)_j - \left(C_{MS-a-WK}\right)_j . \tag{4.19}$$

Compliance compensation is always performed after resistance compensation.

4.3 Results

To evaluate the performance of the proposed parameter estimation method, next we present results for a patient-specific aortic coarctation model extracted from MRI images. In this case, the parameter estimation method ensures that the computational setup is personalized, and, consequently, computed pressure and flow values are in close agreement with the clinical measurements.

Results are reported for four different parameter estimation methods: the calibration method for windkessel parameters (WKC) (Spilker and Taylor 2010), the parameter estimation method with resistance compensation and Direct Compliance compensation (DC), the parameter estimation method with resistance compensation and Analytical Compliance compensation (AC), and the parameter estimation method with resistance compensation and Numerical Compliance compensation (NC).

Blood is modeled as an incompressible Newtonian fluid with a density of 1.050 g/cm^3 and a dynamic viscosity of 0.040 dynes/(cm^2 s). The grid size is 0.05 cm, while the time-step (limited by the CFL-condition) is set equal to 2.5e − 5 s.

Several CFD-based methods for non-invasive assessment of trans-stenotic pressure gradient have been proposed recently (Itu et al. 2013; Keshavarz-Motamed et al. 2011; LaDisa et al. 2011; Ismail et al. 2013a, b). For an accurate patient-specific estimation, the CFD-based solution should be in close agreement with the measured pressure and flow-data, a task that requires automatic calibration of the boundary conditions.

The patient-specific anatomical model (CFD Challenge 2013) is composed of the ascending aorta, three supra-aortic branches, aortic arch, coarctation, and the descending aorta (Fig. 4.3a). Figure 4.3b displays the multiscale model corresponding to the CoA patient-specific geometry. A measured flow rate profile is provided at the inlet, while time-averaged flow-splits are provided for each of the outlets of the geometric model. The objective is to compute the pressure drop across the coarctation, under the constraint that the CFD-based solutions should (1) maintain the same flow-split at each outlet as with the measured data, and (2) replicate the measured systolic and diastolic pressure in the aorta. Figure 4.3c displays the corresponding 0D model.

To build the discretized geometric mesh required for the blood flow computation, we first used the vascular modeling toolkit (VMTK 2014) to extract the centerline

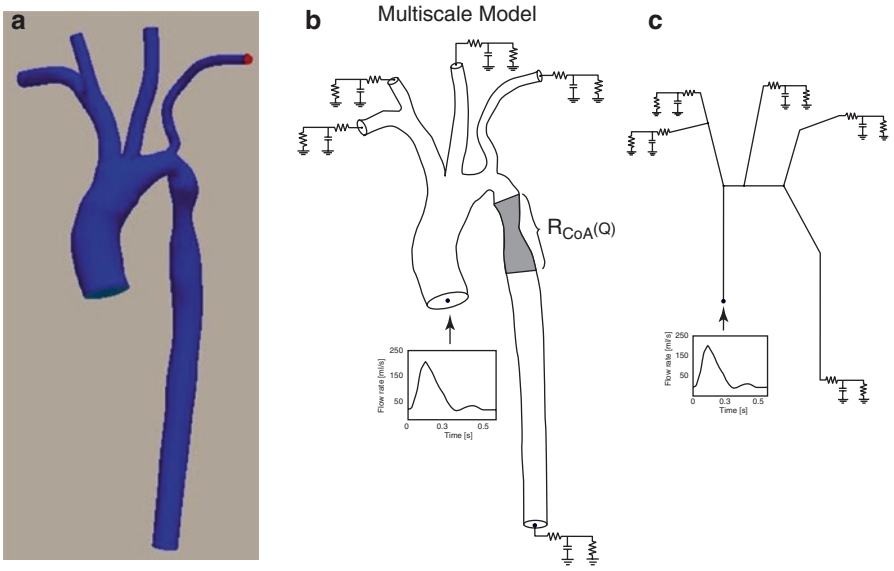

Fig. 4.3 (**a**) Proximal aorta geometry with coarctation, (**b**) Multiscale model used for determining the windkessel parameter values of the patient-specific model, (**c**) 0D model used during the first steps of the model personalization algorithm for finding an initial solution of the parameter values (Itu et al. 2015)

and the cross-sectional areas along the centerline of each arterial segment. Next we used an approach similar to previously introduced ones (Steele et al. 2003), wherein for each vessel of the arterial model, we used several distinct 1D segments with spatially varying cross-sectional area values in order to obtain a geometry close to the 3D geometry acquired through MRI.

Given the high compliance of the ascending aortic wall, this example underlines the advantages of a compliance compensation. At the same time, it also demonstrates the advantages of the resistance compensation for high resistance segments, such as the coarctation.

The parameters to be estimated are the total resistances of the three supra-aortic vessels and of the descending aorta, and the total compliance. The following system of nonlinear equations is numerically solved to obtain the optimum value of each parameter:

$$\mathbf{f}\begin{pmatrix} R_{t-BC} \\ R_{t-LCC} \\ R_{t-LS} \\ R_{t-DAo} \\ C \end{pmatrix} = \begin{Bmatrix} \left(P_{\max}\right)_{comp} - \left(P_{\max}\right)_{ref} \\ \left(P_{\min}\right)_{comp} - \left(P_{\min}\right)_{ref} \\ \left(\Phi_{BC}\right)_{comp} - \left(\Phi_{BC}\right)_{ref} \\ \left(\Phi_{LCC}\right)_{comp} - \left(\Phi_{LCC}\right)_{ref} \\ \left(\Phi_{DAo}\right)_{comp} - \left(\Phi_{DAo}\right)_{ref} \end{Bmatrix} = \begin{Bmatrix} 0 \\ 0 \\ 0 \\ 0 \\ 0 \end{Bmatrix}, \tag{4.20}$$

where P_{max} is the maximum (systolic) pressure, P_{min} is the minimum (diastolic) pressure, (Φ)**.** represents a flow rate split, while $(\bullet)_{comp}$ refers to a value computed using the 0D/Multiscale model, and $(\bullet)_{ref}$ refers to the reference value. Index *BC* refers to the brachiocephalic artery, *LCC* to the left common carotid artery and *DAo* to the descending aorta. The reference systolic and diastolic pressures (115 mmHg and 65 mmHg respectively), and the reference flow-rate splits are taken from literature data (CFD Challenge 2013). Only three of the four flow rate splits are used as objectives in Eq. (4.20) since the fourth one is obtained as difference. The characteristics of the pressure waveform are determined at the outlet of the left subclavian artery (Ismail et al. 2013a, b).

One of the estimated total resistances corresponds to several outlets (R_{t-BC} represents the equivalent total resistance of the right subclavian artery and the right common carotid artery). Hence, before applying Algorithm 1, at the end of the calibration iterations performed for the multiscale model, the total equivalent resistance of the multiscale model at each of the two outlets of the brachiocephalic artery is determined using Eq. (4.12), with a power coefficient equal to two. The proximal resistance of each windkessel model is set equal to the characteristic resistance and was maintained constant throughout the parameter estimation method.

Since total resistance is adapted directly, Algorithm 1 is applied both when switching from the 0D model to the multiscale model, and during each additional calibration iteration performed for the multiscale model. Since compliance is also adapted directly, Eqs. (4.14) and (4.15) are used for the initial compliance compensation, and Eqs. (4.18) and (4.19) are applied at each further calibration iteration.

The objective and parameter values obtained with the four different parameter estimation methods are displayed in Fig. 4.4. Whereas three iterations are required with the WKC method, two iterations are required with the DC and AC methods, and only one iteration is required with the NC method.

With any of the proposed parameter estimation methods, the objective and parameter values are significantly closer to their reference/final values. When the WKC method is used, the pulse pressure at iteration 0 is significantly smaller than the reference pulse pressure, caused by the additional compliance of the highest order model (especially the initial diastolic pressure is considerably closer to the final value). This aspect is also reflected by the fact that the compliance value at iteration 0 is significantly closer to its final value for the proposed methods. Furthermore all initial computed flow rate split values are closer to their final values. This is mainly caused by the significantly improved initial estimate of the total resistance on the descending aorta R_{t-DAo}.

As opposed to the objectives, where the final values are identical for all four parameter estimation methods, the final parameter values are different for the two methods. This is caused by the fact that the herein introduced methods adapt the overall properties of the multiscale model, whereas the WKC method adapts directly the parameters of the three-element windkessel models. Hence, although the parameter values of the two methods at iteration 0 are identical, the values of the windkessel parameters are in fact different. The initial estimate of R_{t-DAo} for the proposed

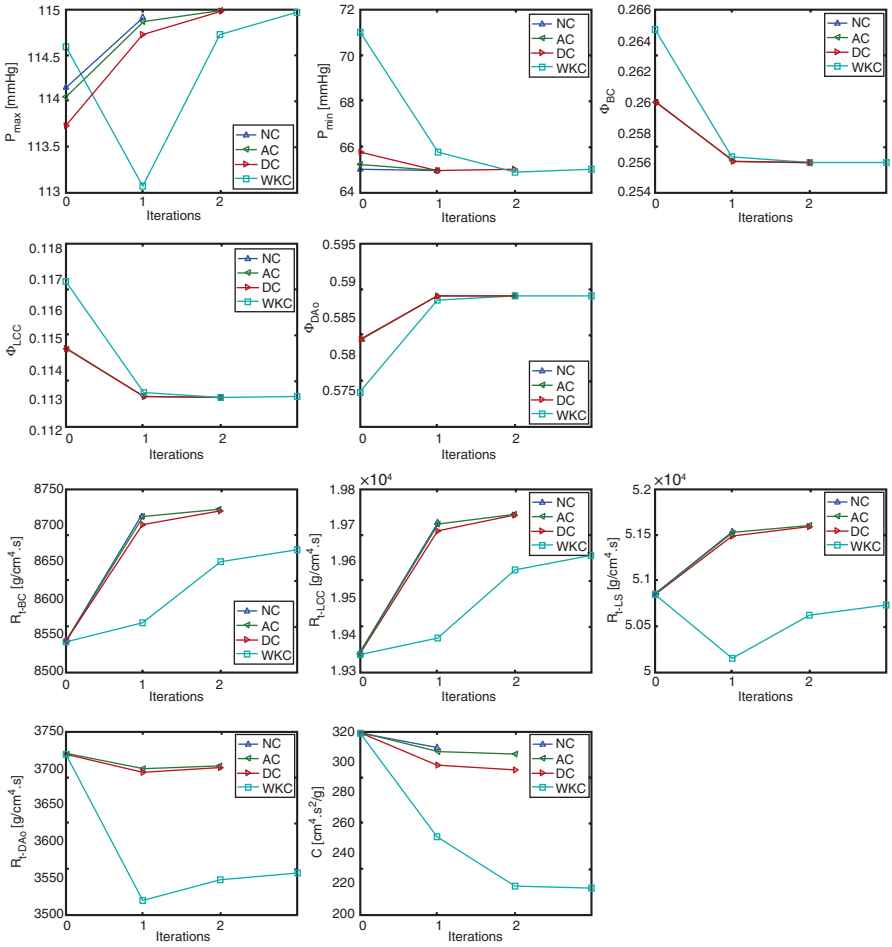

Fig. 4.4 Parameter estimation progression for the proximal aorta model. The total resistance of each of the three supra-aortic branches, the total resistance of the descending aorta windkessel model and the sum of all compliances were the adapted parameters. The desired mean fractions of flow through supra-aortic branches and through the descending aorta were used as objectives, besides systolic and diastolic pressure (Itu et al. 2015)

parameter estimation methods is superior since Eq. (4.11) is employed for computing the resistance of the CoA segment.

Figure 4.5 displays a comparison of the pressure profiles at the outlet of the left subclavian artery, corresponding to the initial solution of the WKC method, the initial solution of the NC method and the final solution (identical for both parameter estimation methods). The initial solution refers to the results obtained at iteration zero with the multiscale model. The initial solution provided by the NC method is clearly superior to the initial solution provided by the WKC method and almost identical to the final solution.

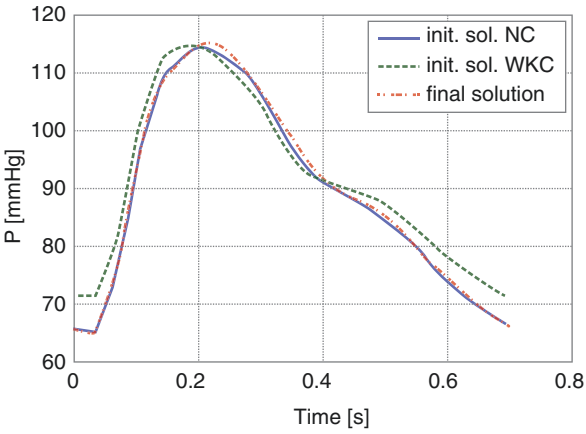

Fig. 4.5 Comparison of the pressure profiles at the outlet of the left subclavian artery of the proximal aorta model, corresponding to the initial solution of the NC method, the initial solution of the WKC method and the final solution (Itu et al. 2015)

Table 4.1 Comparison of reference and computed flow rate split values

Artery	Reference flow split [%]	Computed flow split (NC) [%]
Brachiocephalic artery	25.6	25.6044
Left common carotid artery	11.3	11.3022
Left subclavian artery	4.26	4.3009
Descending aorta	58.8	58.7925

Table 4.2 Final values of the adapted parameters for four different parameter estimation methods applied for the nonlinear system in Eq. (4.20)

Parameter estimation method	$(R_{t\text{-}BC})_{final}$ [g/(cm^4 s)]	$(R_{t\text{-}LCC})_{final}$ [g/(cm^4 s)]	$(R_{t\text{-}LS})_{final}$ [g/(cm^4 s)]	$(R_{t\text{-}DAo})_{final}$ [g/(cm^4 s)]	$(C)_{final}$ [10^{-6} cm^4 s^2/g]
NC	8711.3	19,710.6	51,541.6	3698.0	308.71
AC	8720.0	19,730.8	51,595.4	3700.7	304.63
DC	8718,8	19,728.2	51,587.6	3700.0	294.18
WKC	8665.7	19,615.9	50,715.9	3555.4	216.14

Table 4.1 compares the reference and the computed flow rate split values (obtained with the NC method): the values match almost perfectly. Tables 4.2 and 4.3 display for each parameter estimation method the final values of the adapted parameters and the compensated multiscale compliance and CoA resistance values respectively. The compensated compliance is highest for the NC method. Importantly, the sum of the five compensated compliance values reflects the difference between the final total compliance values obtained with the proposed parameter estimation methods and with the WKC method. Furthermore, the compensated CoA resistance (R_{CoA}) roughly reflects the difference between the final total resistance value on the descending aorta ($R_{t\text{-}DAo}$) obtained with the proposed methods and with the WKC method.

Table 4.3 Compensated CoA resistance and compliance values for four different parameter estimation methods applied for the nonlinear system in Eq. (4.20)

Parameter estimation method	R_{CoA} [g/(cm^4 s)]	$C_{MS\text{-}a\text{-}WK}$ [10^{-6} cm^4 s^2/g]				
		RS	RCC	LCC	LS	DAo
NC	125.17	18.15	9.679	13.23	5.830	45.68
AC	125.17	17.45	0.245	12.77	5.442	44.37
DC	125.17	15.44	8.097	11.48	4.700	38.85
WKC	0.0	0.0	0.0	0.0	0.0	0.0

RS right subclavian artery, *RCC* right common carotid artery, *LCC* left common carotid artery, *LS* left subclavian artery

The computed average pressure drop across the coarctation is 4.12 mmHg, while the peak pressure difference is of 16.88 mmHg, both in the range of the values reported for the challenge (Ismail et al. 2013a, b).

4.4 Discussion

The results presented in the previous section demonstrate the potential advantages of the model personalization algorithm, which leads to superior calibration results for the considered patient-specific CoA geometry. The DC and AC methods are easier to implement and computationally faster due to their analytical nature. Given the high computational cost associated with multiscale models, the additional execution time for the NC method, compared to the DC and AC methods, is negligible. Since the NC method has the best performance, we consider this variant of the proposed parameter estimation method to be the most efficient. Note that the configurations of the 0D model and the multiscale model are not affected by the additional steps in the proposed parameter estimation method, and the framework developed for the WKC method can be completely reused.

The geometrical multiscale framework for the aortic model is useful for modeling multiple pathologies. Recently, we validated (with in-vivo measurements) a reduced-order multiscale model for the non-invasive assessment of aortic coarctation (Itu et al. 2013). A fully automated parameter estimation method was proposed for personalizing the hemodynamic computations. The goals of this estimation method were to match the patient-specific average aortic pressure, the flow distribution between supra-aortic arteries and the descending aorta, and to determine the aortic wall properties. Promising validation results were obtained for the non-invasive computation of the trans-coarctation peak-to-peak pressure-gradient.

The configuration used in the previous section for the CoA geometry provides the possibility to enhance the personalization of the hemodynamic computations by matching not necessarily the mean arterial pressure, computed from the systolic and diastolic pressure, but directly the two cuff-based pressures. Matching the flow rate split for the descending aorta is crucial since the trans-coarctation pressure-drop is highly dependent on the flow rate through the descending aorta. Previously only the

average flow rate was considered, but, using an automated parameter estimation method, the maximum and/or minimum flow rate can also be constrained.

The proposed parameter estimation method could potentially provide significant advantages when the multiscale model is an FSI model (when rigid wall models are used, only the resistance compensation is required). For the non-invasive assessment of aortic coarctation FSI modeling is required: since the trans-coarctation pressure gradient is computed as a peak-to-peak pressure difference between the ascending aorta and the descending aorta, the pressure drop is not mainly determined by the maximum flow rate and the geometry, but by the complex interaction between these two aspects, the phase lag introduced by the compliance, the wave propagation speed, and the backward travelling pressure and flow rate waves. Furthermore, the wall properties can also be used as adapted parameters in order to match a specific feature of the wave propagation aspects.

Parameter estimation methods for model personalization are not only useful for performing patient-specific computations using measured data, but also to perform computations for other conditions, like exercise, drug-induced hyperemia, or post surgical intervention. Patient-specific computations for CoA patients corresponding to the exercise state were reported previously (LaDisa et al. 2011), where time-varying and average trans-coarctation pressure gradient, wall shear stress and oscillatory shear index parameters were analyzed. Parameter estimation methods may provide the possibility to enhance the value of such (predictive) computations by imposing different changes for the reference values, compared to the rest state. For example, different elevations of mean or systolic aortic pressure, or of flow rate through the descending aorta could be imposed. After further evaluation and clinical research, such an approach could have the potential to eliminate the risks and the costs involved in measuring these quantities in-vivo. Regarding treatment planning evaluation, parameter estimation methods could be useful for imposing a certain post-interventional state for the hemodynamic computation, which could then enable an accurate assessment of the treatment options.

References

Alastruey J, Khir A, Matthys K, Segers P, Sherwin S, Verdonck P, Parker K, Peiro J (2011) Pulse wave propagation in a model human arterial network: assessment of 1-D visco-elastic simulations against in vitro measurements. J Biomech 44:2250–2258. doi:10.1016/j.jbiomech.2011.05.041

Bertoglio C, Moireau P, Gerbeau J-F (2012) Sequential parameter estimation for fluid–structure problems: application to hemodynamics. Int J Numer Method Biomed Eng 28:434–455. doi:10.1002/cnm.1476

Bessems D (2007) On the propagation of pressure and flow waves through the patient-specific arterial system. PhD Thesis, TU Eindhoven, Netherlands

Blanco PJ, Watanabe SM, Feijo RA (2012) Identification of vascular territory resistances in one-dimensional hemodynamics simulations. J Biomech 45:2066–2073. doi:10.1016/j.jbiomech.2012.06.002

Cebral JR, Mut F, Weir J, Putman CM (2011) Association of hemodynamic characteristics and cerebral aneurysm rupture. Am J Neuroradiol 32:264–270. doi:10.3174/ajnr.A2274

CFD Challenge (2013) Simulation of hemodynamics in a patient-specific aortic coarctation model. http://www.vascularmodel.org/miccai2012/. Accessed 15 June 2013

Formaggia L, Lamponi D, Quarteroni A (2003) One dimensional models for blood flow in arteries. J Eng Math 47:251–276. doi:10.1023/B:ENGI.0000007980.01347.29

Grinberg L, Karniadakis GE (2008) Outflow boundary conditions for arterial networks with multiple outlets. Ann Biomed Eng 36:1496–1514. doi:10.1007/s10439-008-9527-7

Haggerty CM, Kanter KR, Restrepo M, de Zelicourt DA, Parks WJ, Rossignac J, Fogel MA, Yoganathan AP (2013) Simulating hemodynamics of the Fontan y-graft based on patient-specific in vivo connections. J Thorac Cardiovasc Surg 145:663–670. doi:10.1016/j.jtcvs.2012.03.076

Hom JJ, Ordovas K, Reddy GP (2008) Velocity-encoded cine MR imaging in aortic coarctation: functional assessment of hemodynamic events. Radiographics 28:407–416

Huo Y, Svendsen M, Choy JS, Zhang ZD, Kassab GS (2012) A validated predictive model of coronary fractional flow reserve. J R Soc Interface 9:1325–1338. doi:10.1098/rsif.2011.0605

Ismail M, Gee MW, Wall WA (2013a) CFD challenge: hemodynamic simulation of a patient-specific aortic coarctation model with adjoint-based calibrated windkessel elements. Lect Notes Comput Sci 7746:44–52. doi:10.1007/978-3-642-36961-2_6

Ismail M, Wall WA, Gee MW (2013b) Adjoint-based inverse analysis of windkessel parameters for patient-specific vascular models. J Comput Phys 244:113–130. doi:10.1016/j.jcp.2012.10.028

Itu L, Sharma P, Mihalef V, Kamen A, Suciu C, Comaniciu D (2012) A patient-specific reduced-order model for coronary circulation. In: Proceedings of the international symposium on biomedical imaging, Barcelona, Spain, pp 832–835. doi: 10.1109/ISBI.2012.6235677

Itu L, Sharma P, Ralovich K, Mihalef V, Ionasec R, Everett A, Ringel R, Kamen A, Comaniciu D (2013) Non-invasive hemodynamic assessment of aortic coarctation: validation with in vivo measurements. Ann Biomed Eng 41:669–681. doi:10.1007/s10439-012-0715-0

Itu L, Sharma P, Passerini T, Kamen A, Suciu C, Comaniciu D (2015) A parameter estimation framework for patient-specific hemodynamic computations. J Comput Phys 281:316–333

Keshavarz-Motamed Z, Garcia J, Pibarot P, Larose E, Kadem L (2011) Modeling the impact of concomitant aortic stenosis and coarctation of the aorta on left ventricular workload. J Biomech 44:2817–2825. doi:10.1016/j.jbiomech.2011.08.00

LaDisa JFJ, Figueroa CA, Vignon-Clementel IE, Kim HJ, Xiao N, Ellwein LM, Chan FP, Feinstein JA, Taylor CA (2011) Computational simulations for aortic coarctation: representative results from a sampling of patients. J Biomech Eng 133:091008. doi:10.1115/1.4004996

Low K, van Loon R, Sazonov I, Bevan RLT, Nithiarasu P (2012) An improved baseline model for a human arterial network to study the impact of aneurysms on pressure-flow waveforms. Int J Numer Method Biomed Eng 28:1224–1246. doi:10.1002/cnm.2533

Malossi C, Blanco P, Deparis S (2012) A two-level time step technique for the partitioned solution of one-dimensional arterial networks. Comput Methods Appl Mech Eng 237:212–226. doi:10.1016/j.cma.2012.05.017

Moireau P, Bertoglio C, Xiao N, Figueroa CA, Taylor CA, Chapelle D, Gerbeau JF (2013) Sequential identification of boundary support parameters in a fluid-structure vascular model using patient image data. Biomech Model Mechanobiol 12:475–496. doi:10.1007/s10237-012-0418-3

Murray CD (1926) The physiological principle of minimum work: I. The vascular system and the cost of blood volume. Proc Natl Acad Sci U S A 12:207–214

Mynard JP, Nithiarasu P (2008) A 1D arterial blood flow model incorporating ventricular pressure, aortic valve and regional coronary flow using the locally conservative Galerkin (LCG) method. Int J Numer Method Biomed Eng 24:367–417. doi:10.1002/cnm.1117

Mynard JP, Davidson MR, Penny DJ, Smolich JJ (2012) A simple, versatile valve model for use in lumped parameter and one-dimensional cardiovascular models. Int J Numer Method Biomed Eng 28:626–641. doi:10.1002/cnm.1466

Olufsen M, Peskin C, Kim WY, Pedersen EM, Nadim A, Larsen J (2000) Numerical simulation and experimental validation of blood flow in arteries with structured-tree outflow conditions. Ann Biomed Eng 28:1281–1299. doi:10.1114/1.1326031

Olufsen MS, Nadim A, Lipsitz LA (2002) Dynamics of cerebral blood flow regulation explained using a lumped parameter model. Am J Physiol Regul Integr Comp Physiol 282:611–622. doi:10.1152/ajpregu.00285.2001

Pant S, Fabrèges B, Gerbeau J-F, Vignon-Clementel IE (2014) A multiscale filtering-based parameter estimation method for patient-specific coarctation simulations in rest and exercise, Statistical Atlases and Computational Models of the Heart. Imaging and Modelling Challenges. Lect Notes Comput Sci 8330:102–109. doi:10.1007/978-3-642-54268-8_12

Quarteroni A, Tuveri M, Veneziani A (2000) Computational vascular fluid dynamics: problems, models and methods. Comput Vis Sci 2:163–197. doi:10.1007/s007910050039

Raghu R, Vignon-Clementel I, Figueroa CA, Taylor CA (2011) Comparative study of viscoelastic arterial wall models in nonlinear one-dimensional finite element simulations of blood flow. J Biomech Eng 133:081003. doi:10.1115/1.4004532

Reymond P, Bohraus Y, Perren F, Lazeyras F, Stergiopulos N (2011) Validation of a patient-specific one-dimensional model of the systemic arterial tree. Am J Physiol Heart Circ Physiol 301:1173–1182. doi:10.1152/ajpheart.00821.2010

Ringel RE, Jenkins K 2007 Coarctation of the aorta stent trial (coast). http://clinicaltrials.gov/ct2/show/NCT00552812. Accessed 10 Mar 2012

Seifert BL, DesRochers K, Ta M, Giraud G, Zarandi M, Gharib M, Sahn DJ (1999) Accuracy of Doppler methods for estimating peak-to-peak and peak instantaneous gradients across coarctation of the aorta: an in vitro study. J Am Soc Echocardiogr 12:744–753

Spilker R, Taylor CA (2010) Tuning multidomain hemodynamic simulations to match physiological measurements. Ann Biomed Eng 38:2635–2648. doi:10.1007/s10439-010-0011-9

Steele BN (2007) Using one-dimensional finite element analysis to estimate differential pressure of renal artery stenoses. In: Proceedings of computer in cardiology, Durham, NC, USA, pp 381–384. doi: 10.1109/CIC.2007.4745504

Steele BN, Wan J, Ku JP, Hughes TJR, Taylor CA (2003) In vivo validation of a one-dimensional finite-element method for predicting blood flow in cardiovascular bypass grafts. IEEE Trans Biomed Eng 50:649–656. doi:10.1109/TBME.2003.812201

Stergiopulos N, Young DF, Rogge TR (1992) Computer simulation of arterial flow with applications to arterial and aortic stenosis. J Biomech 25:1477–1488. doi:10.1016/0021-9290(92)90060-E.

Stergiopulos N, Meister JJ, Westerhof N (1994) Simple and accurate way for estimating total and segmental arterial compliance: the pulse pressure method. Ann Biomed Eng 22:392–397. doi:10.1007/BF02368245

Taylor CA, Steinman DA (2010) Image-based modeling of blood flow and vessel wall dynamics: applications, methods and future directions. Ann Biomed Eng 38:1188–1203. doi:10.1007/s10439-010-9901-0

The Vasular Modeling Toolkit (2014) http://www.vmtk.org/. Accessed 1 May 2014

Westerhof N, Lankhaar JW, Westerhof BE (2009) The arterial windkessel. Med Biol Eng Comput 47:131–141. doi:10.1007/s11517-008-0359-2

Womersley JR (1955) Method for the calculation of velocity, rate of flow and viscous drag in arteries when the pressure gradient is known. J Physiol 127:553–563

Young DF, Cholvin NR, Roth AC (1975) Pressure drop across artificially induced stenoses in the femoral arteries of dogs. Circ Res 36:735–743

Zamir M, Sinclair P, Wonnacott TH (1992) Relation between diameter and flow in major branches of the arch of the aorta. J Biomech 25:1303–1310. doi:10.1016/0021-9290(92)90285-9